

Short Communication

Structural Modification, Synthesis Mechanism and Properties Analysis of $\text{Li}_4\text{Ti}_5\text{O}_{12}$ Anode Materials

Cheng Liu, Ju Rong, Yannan Zhang, Xiaohua Yu*, Jianxiong Liu*, Zhaolin Zhan

Faculty of Materials Science and Engineering, Kunming University of Science and Technology, Kunming, 650093, P.R.China.

*E-mail: xiaohua_y@163.com, ljx5192665@163.com

Received: 2 June 2017 / Accepted: 2 August 2017 / Published: 12 September 2017

$\text{Li}_4\text{Ti}_5\text{O}_{12}$ microsphere was synthesized by hydrothermal method. The effects of amount of lithium hydroxide, hydrothermal time and sintering temperature on properties of sample were studied. The synthesis mechanism of $\text{Li}_4\text{Ti}_5\text{O}_{12}$ microsphere was preliminary analyzed. The structural characterization was analyzed by X-ray diffraction, and the morphology was investigated by scanning electron microscopy and transmission electron microscopy. The properties of galvanostatic charge, discharge and cycle stability were also studied. The results indicated that when 2.55 mmol $\text{LiOH}\cdot\text{H}_2\text{O}$ reacted with 0.2 g hydrolysate, the sample had pure phase, when the hydrothermal condition was 36 h and 180 °C, the structure of sample particle was intactly spherical. The volume average size of samples were between 400 nm to 600 nm. The charge and discharge voltage plateau of samples were very stable. When the sintering temperature was 700 °C, the first discharge capacity was 148.3 $\text{mAh}\cdot\text{g}^{-1}$ at 0.1 C. After 10th cycle, the discharge capacity retained at 132.5 $\text{mAh}\cdot\text{g}^{-1}$.

Keywords: Lithium titanate; hydrothermal condition; electrochemical property; hydrothermal method

1. INTRODUCTION

Spinel $\text{Li}_4\text{Ti}_5\text{O}_{12}$ is one of the hot spots in lithium ion battery anode material research due to its zero strain effect, stable charge and discharge platform, as well as good cycle stability [1,2]. These good features offer an attractive option for a lot applications, especially where high safety and reliability is required such as hybrid electric vehicles and electric vehicles [3,4]. However, the inherent defects such as low conductivity and low capacity also hindered its large-scale application. Currently, many studies are mainly focusing on the modification of $\text{Li}_4\text{Ti}_5\text{O}_{12}$, the strategies include metal ion doping [5,6], adding conductive agent [7,8], structural modification [9-11] and so on.

For $\text{Li}_4\text{Ti}_5\text{O}_{12}$, structural modification is one of the effective ways to improve its electrochemical performance and keep its “zero-strain” characteristic [12,13]. The special shape can not only improve the bulk density of the powder, but also retain a high specific surface area. As a result, high rate of lithium ion diffusion can be maintained in the case of high current discharge, the electrode polarization is inhibited, and capacity loss is reduced. So many studies have focused on the preparation of special shapes of $\text{Li}_4\text{Ti}_5\text{O}_{12}$, such as sheet structures [11,14], three-dimensional ordered porous structures [15], nanowires/tube structures [16,17], hollow sphere structures [18] and so on. No wonder almost all the structures above are nano-sized, surface effect of nanomaterial ensure a high specific surface area of them. The main synthetic methods are hydrothermal method [19-21], template method [17], Sol-gel method [22,23] and so on. Liquid-liquid interface between two immiscible liquids could give a very unique non-equilibrium reaction environment with high surface energy, which may lead to complex crystallization processes and interesting materials [24,25]. In this work, $\text{Li}_4\text{Ti}_5\text{O}_{12}$ microspheres with spinel structure were synthesized by hydrothermal method using tetrabutyl titanate, lithium hydroxide and absolute ethanol. The synthesis conditions were optimized and synthesis mechanism of $\text{Li}_4\text{Ti}_5\text{O}_{12}$ microsphere was preliminary analyzed.

2. EXPERIMENTAL

2.1. Synthesis

A mixture of 200 ml absolute ethanol and 0.8 ml 0.1mol/L KCl solution was homogeneously mixed. The 8.80 g of tetrabutyl titanate (TBT) was added dropwise to the above mixture under ultrasonic conditions, and ultrasonic vibration was continued for 10 minutes to obtain white precipitate. The suspension was slowly stirred for 6 hours and aged at room temperature for 24 hours, after centrifugation and washed by alcohol for several times, the sedimentation of the sample was drying at 60 °C. A certain amount of $\text{LiOH}\cdot\text{H}_2\text{O}$ was added to a mixture of 30 mL of ethanol-water ($V(\text{A})/V(\text{B}) = 1: 1$). 0.2 g of hydrolyzate was added and stirring was continued for 10 min. Then it was transferred into a PTFE-lined autoclave at 180 °C for a certain period of time. After cooling naturally, the light yellow precipitate was separated by filtration, followed by washing and vacuum drying at 60 °C. Finally, the dried precipitate was sintered under a certain temperature conditions.

2.2. Material characterization

The phase structure of the samples was analyzed by PHILIPS X'Pert Pro X-ray diffraction (XRD) with Cu-K α radiation at scanning rate of 8°min^{-1} , and the diffraction patterns were recorded in the angle (2θ) range from 10° to 80° . The grain size of the sample was calculated by Scherrer formula [26], that is, $D = K\lambda / \beta \cos\theta$, where: D is the grain size (nm), K is the Scherrer constant, λ is the X-ray wavelength, B is the integral half-height width, and θ is the diffraction angle. The shape of the sample was observed with a JSM-6700F field emission scanning electron microscope (FE-SEM) and a Tecnai G² 20 S-TWIN type transmission electron microscopy (TEM) appearance. The secondary particle size

and particle size distribution of the powder samples were tested with a MALVERN Zetasizer 3000HSA particle size analyzer.

2.3. Electrochemical measurement

CR2025-type coin cells were assembled in an argon-filled glovebox in which both oxygen and water concentrations were less than 1 ppm. In the cell, pure lithium sheet acted as the reference and counter electrode. The working electrode was composed of active material, acetylene black as conducting agent, polyvinylidene fluoride (PVDF) as binder dissolved in N-methyl pyrrolidinone (NMP) and the mass ratio of the three matters was 85:7:8. The mixture was grinded in a carnelian mortar for 1 hour to be a slurry substance. The slurry was uniformly coated on an aluminum foil having a thickness of 20 μm , dried at 60 $^{\circ}\text{C}$, pressed with a roll machine, dried at 120 $^{\circ}\text{C}$ for 10 hours, and cut into small pieces of $\Phi 12$ mm. The electrolyte used in the cell was of 1 M LiPF₆ in a mixing solvent of ethylene carbonate (EC) and diethyl carbonate by the volume ratio of 1:1. The galvanostatic charge-discharge measurement was conducted on Land battery test system (LAND CT2001A) by Wuhan Jinnuo Electronics Co., Ltd with the voltage range from 1.0 to 2.5 V at room temperature.

3. RESULTS AND DISCUSSION

Figure 1 shows the XRD patterns of different amounts of lithium hydroxide hydrothermal at 180 $^{\circ}\text{C}$ for 12 h and heat treatment at 600 $^{\circ}\text{C}$ for 1 h. It can be seen from Fig.1 that when the amount of lithium hydroxide is 2.0 mmol, the main crystal phase of the sample is Li₄Ti₅O₁₂, anatase TiO₂ and rutile TiO₂. It can be seen that the amount of LiOH is insufficient during the hydrothermal process. The excess amount of hydrated TiO₂ is hydrolyzed to form anatase or rutile TiO₂ during the sintering. Similar phenomena also appear in research of Liu [27] and Sha [28].

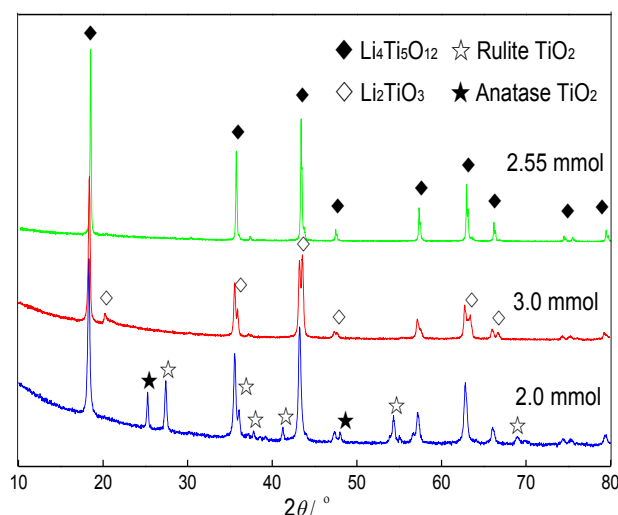


Figure 1. X-ray diffraction pattern of samples synthesized at different amounts of lithium hydroxide hydrothermal at 180 $^{\circ}\text{C}$ for 12 h and sintering at 600 $^{\circ}\text{C}$ for 1 h.

When the amount of lithium hydroxide is 3.0 mmol, the main crystal phase of the sample is $\text{Li}_4\text{Ti}_5\text{O}_{12}$ and Li_2TiO_3 . It is evidently that lithium hydroxide is excessive, so excess Li atoms combine with Ti atoms to form Li_2TiO_3 . Some studies show that its necessary for excess of lithium hydroxide, but the key is to control the level of excess[29-31]. When the amount of lithium hydroxide is 2.55 mmol, the sample is pure phase $\text{Li}_4\text{Ti}_5\text{O}_{12}$, no other heterogeneous peaks. In summary, when the amount of lithium hydroxide is 2.55 mmol, there is no miscellaneous phase. So it is applied as optimum amount of lithium hydroxide in the following experiment.

Figure 2 is the SEM image of the sample hydrothermal at 180 °C for 12 h, 24 h, 36 h and heat treatment at 600 °C for 1 h. It is well known that hydrothermal time make a great difference to sample morphology. Many researcher obtain different shape under different hydrothermal time, such as hollow microsphere [30], mesoporous microsphere [31], sawtooth-like nanosheets [32] and nanotubes [33]. After hydrothermal for 12 h, the sample does not appear spherical morphology, but formed by the accumulation of small sheet. It is noticed that individual places have a trend to formed a spherical, it is consistent with Shao's work[28]. When the hydrothermal time is extended to 24 h, the most of sample have a spherical morphology, and the dispersion is more uniform. However, there are still sheet shape inside, the surface is more rough, individual balls stick together, the diameter of 400-700 nm. Compared with study of Wang [34], sphere of $\text{Li}_4\text{Ti}_5\text{O}_{12}$ is much faster here, this may attribute to higher temperature accelerate the diffusion process. When the hydrothermal time is 36 h, the sample morphology is almost all spherical, the ball surface is also very rough, but the dispersion is better, basically no bonding, the diameter is also around 400-700 nm. Likely, it is applied as optimum hydrothermal time in the following experiment.

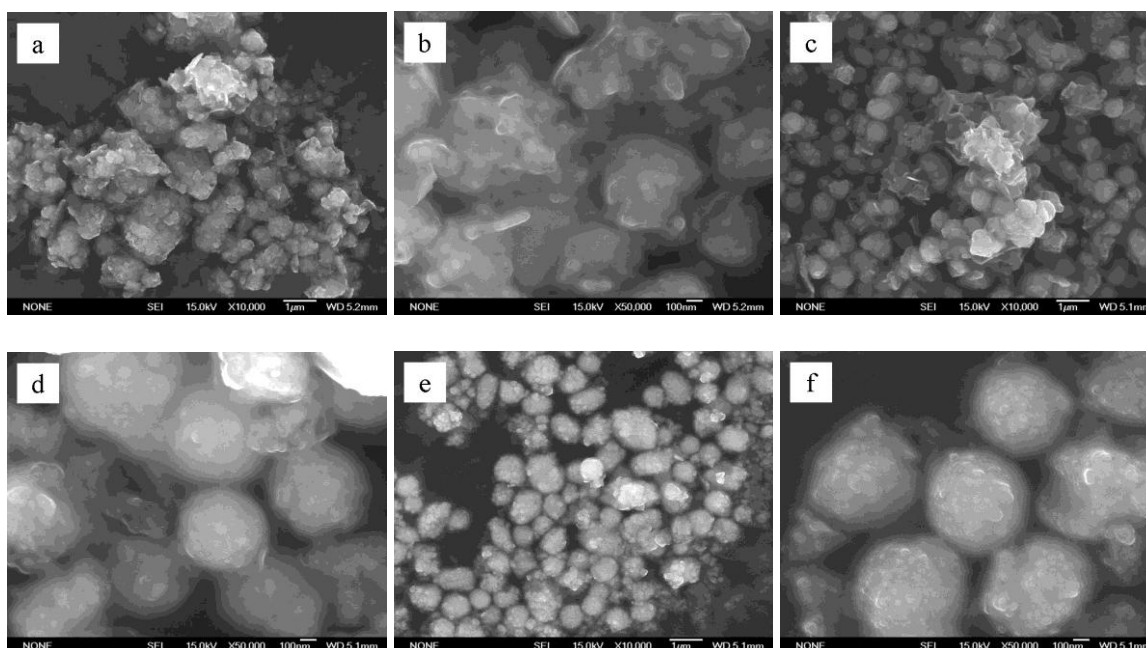


Figure 2. SEM images of samples synthesized at different hydrothermal time when the amount of lithium hydroxide is 2.55 mmol and sintering at 600 °C for 1 h, a and b hydrothermal for 12 h, c and d hydrothermal for 24 h, e and f hydrothermal for 36 h

It can be seen that with the extension of the hydrothermal time, the spherical structure is getting better and better. When the hydrothermal time is short, the sample is mostly irregular sheet. After the extension of the hydrothermal time, the sheet gradually disappear, replaced by monodisperse microspheres, which is due to particles gather more closely to maintain a good spherical shape during longer hydrothermal process. Therefore, 36 h is the appropriate hydrothermal time.

Figure 3 shows the XRD patterns of samples obtained at different heat treatment temperatures for 1 h after 36 h hydrothermal process. It can be seen from figure 3 that the samples are pure phase $\text{Li}_4\text{Ti}_5\text{O}_{12}$ (JCPDS no. 49-0207), no miscellaneous phase appears. The peak width of sample is large at 500 °C. With the temperature rise, $\text{Li}_4\text{Ti}_5\text{O}_{12}$ diffraction peak strength is higher and higher. The peak becomes more and more sharp, indicating that with the temperature rise, the crystal development of the sample is getting better and better. In Wu’s work [36], the heat treatment is at 450 °C, 550 °C, 650 °C and 750 °C. Similar law is confirmed.

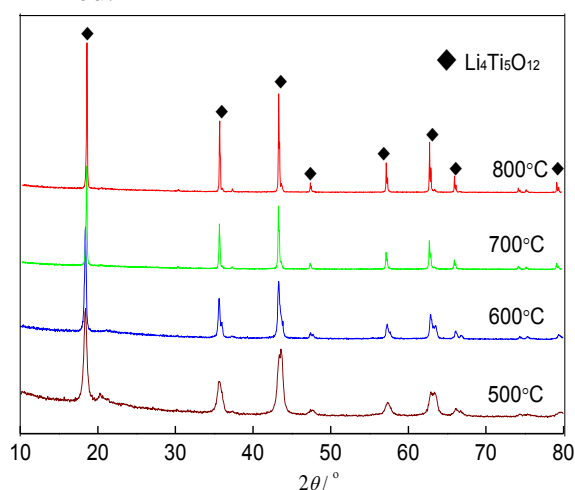


Figure 3. X-ray diffraction pattern of samples synthesized at different sintering temperatures for 1 h after 36 h hydrothermal process

Table 1. The grain size and particle size distribution of samples synthesized at different sintering temperatures for 1 h after 36 h hydrothermal process

Sintering Temperature /°C	Grain size /nm	Volume average size /nm	Particle size distribution /nm
500	22.12	449.4	146.4-734.5
600	36.97	525.8	84.7-673.8
700	63.27	530.3	135.4-679.3
800	67.15	555.7	141.0-890.6

Table 1 shows the grain size, average volume particle size and particle size distribution of the sample. It can be seen that the grain size of the sample increases with the increase of temperature, indicating that with the increase of temperature, the crystal development of the sample is better and the grain grows. The volume average particle size of the sample is about 400-600nm and the particle size

distribution is 100-900 nm, which is consistent with the SEM results in figure 2. Particle size of sample at 800 °C has tendency to increase, the sample size distribution range is the largest. May be the temperature rise, making the material diffusion intensified, so the particles grow.

The synthesis of lithium titanate microspheres can be roughly divided into three steps: the hydrolysis of tetrabutyl titanate, the hydrothermal process and the heat treatment process.

Figure 4 shows the XRD pattern of the tetrabutyl titanate hydrolyzate after drying at 60 °C. The hydrolyzate shown in the figure is substantially amorphous. There is weak diffraction peak at $2\theta = 25.14^\circ$, 37.98° , 49.40° , 55.36° . Compared with the standard spectrum (JCPDS no. 83-2243), the diffraction peak is consistent with anatase TiO_2 . In combination with the experimental results and literature [37-38]. It is presumed that $\text{Ti}(\text{C}_4\text{H}_9\text{O})_4$ is first hydrolyzed into hydrated $[\text{TiO}_6]$ octahedron in the first stage with Ti-OH group structure; the presence of Cl^- makes the Ti^- protonated to form Ti-OH_2^+ . These protonated surfaces are easily combined with other hydrated $[\text{TiO}_6]$ octahedral-OH, which lacks a water molecule to form a Ti-O-Ti oxide bridge-bound system in which the coplanar structure occurs during hydration $[\text{TiO}_6]$ octahedral formation of amorphous hydrated anatase phase TiO_2 microspheres.

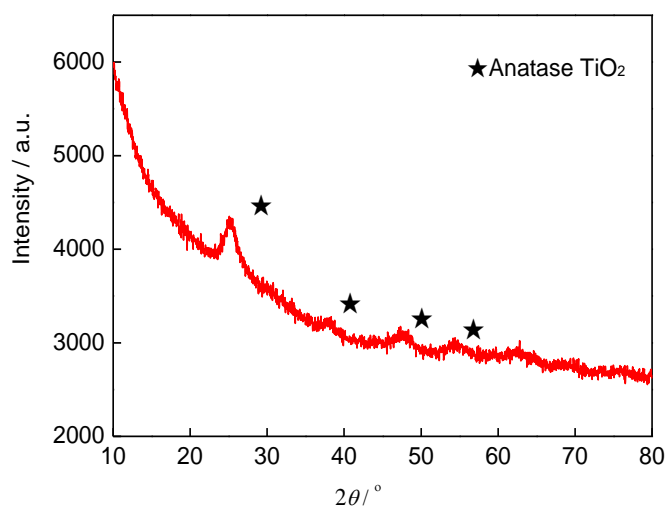


Figure 4. X-ray diffraction pattern of hydrolyzate after drying at 60 °C

Figure 5 shows the XRD pattern of the sample hydrothermal reaction for 36 h without heat treatment. It can be seen that LiTiO_2 and complex hydrate titanium oxide appear in the process of hydrothermal process, the crystallinity is poor and the diffraction peak is weak. It is also speculated that in the process of hydrothermal, adding LiOH ethanol-water solution, OH^- and H_2O may enter the hydrated TiO_2 microspheres, and the combination of titanium ions or lattice oxygen may form HTiO_3^- structure, and Li^+ and HTiO_3^- combine to form Li-Ti-H-O complex system [38].

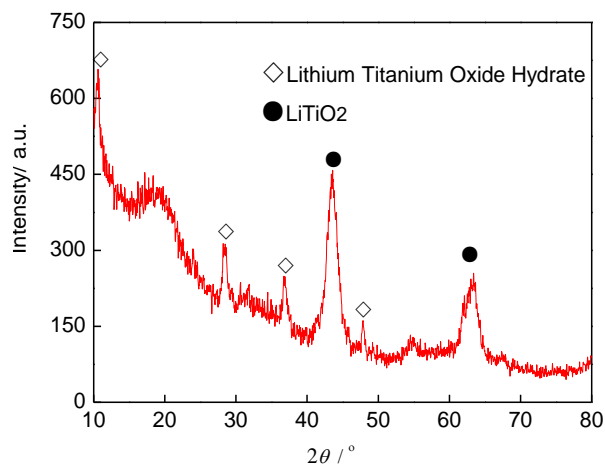


Figure 5. X-ray diffraction pattern of hydrothermal products without sintering

In the final stage, the heat treatment causes the H_2O in the hydrothermal product to be lost, while the original phase is recrystallized at a higher temperature to form $Li_4Ti_5O_{12}$.

Combined with the result of XRD above, the hydrothermal process can be described briefly. Under the condition of KCl, the hydrated TiO_2 microspheres are formed by hydrolysis of tetrabutyl titanate:



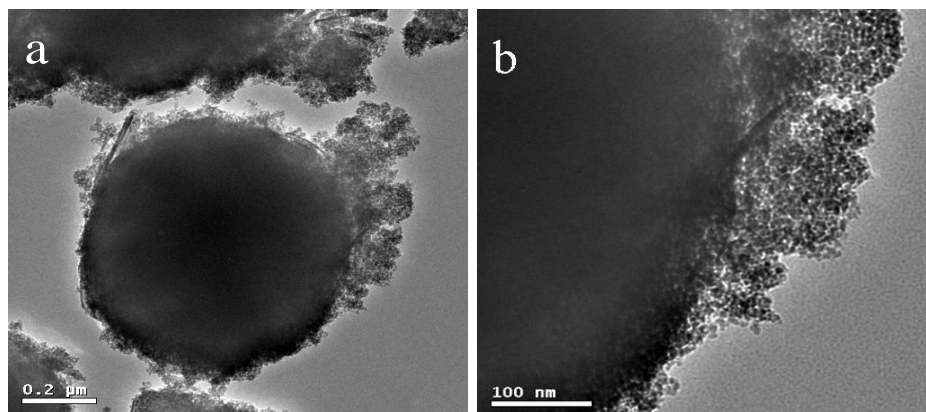
Lithium inserts into the TiO_2 can form mesophase lithium titanium oxide:



Further reaction of mesophase lithium titanium oxide and TiO_2 can form the precursor of $Li_4Ti_5O_{12}$ phase. Li^+ is reacted with cation in hydrated TiO_2 microspheres. The $Li-Ti-H_2O$ system was formed by the substitution reaction:



Figure 6 is TEM images of samples before and after heat treatment. From Fig. 6a and 6c, it can be seen that the size of the sample after the hydrothermal process is about 600 nm, and the size of the sample is not changed after heat treatment. As can be seen from Fig. 6b and 6d, many tiny particles are attached to the surface of the spherical particles.



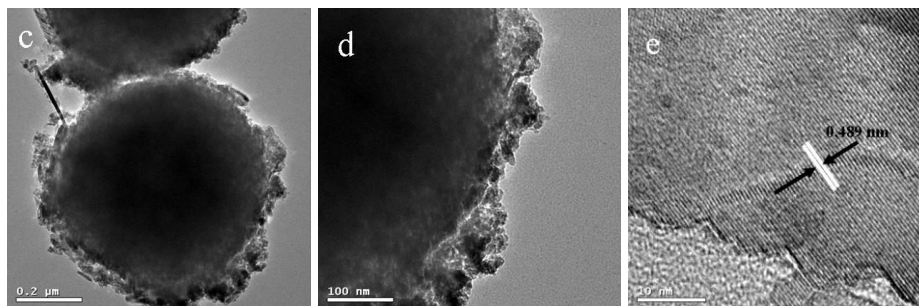


Figure 6. TEM images of samples before and after sintering. a,b is the TEM of the sample hydrothermal at 180 °C for 36 h without sintering, c, d and e are the TEM of the sample sintering at 600 °C for 1 h under the same conditions.

There are some small gaps before the heat treatment. After heat treatment, small particles seem more fluffy, more compact, and the gap is reduced, indicating that the heat treatment process appeared dense. Figure 6e is high magnification TEM picture of the sample. We can get the surface spacing of about 0.489 nm by calculation. Comparison with the standard spectrum (JCPDS no. 26-1198), it is very close to $\text{Li}_4\text{Ti}_5\text{O}_{12}$ d (111) = 0.483nm. This means that the sample is pure phase $\text{Li}_4\text{Ti}_5\text{O}_{12}$, which is consistent with the previous XRD results. It is known that the size of spherical particles is not changed during the formation of lithium titanate microspheres. The spherical particles are composed of many smaller particles with a size of about 10-40nm, and the heat treatment process makes the microspheres denser.

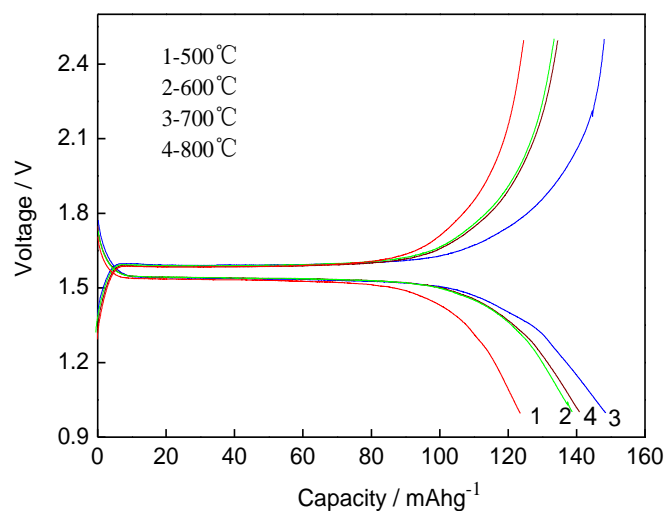


Figure 7. The first charge and discharge curves for the samples synthesized at different sintering temperatures

Figure 7 shows the initial charge-discharge curves at 0.1C for samples with different heat treatment temperatures. 1, 2, 3, 4 are the first charge and discharge curves of 1h samples after 500 °C, 600 °C, 700 °C and 800 °C heat treatment. It can be seen from Fig.7 that the first discharge specific capacity of the samples prepared by heat treatment at 500 °C, 600 °C, 700 °C and 800 °C for 1 hour is

123.5, 138.5, 148.3 and 140.9 mAh·g⁻¹, respectively. All the charge and discharge curves are very obvious and stable charge and discharge voltage platform. Charge and discharge voltage were 1.60V and 1.55V respectively. The voltage difference is very small, indicating that the charge and discharge process reversible degree is better. For sample with 700 °C heat treatment, the first discharge capacity of up to 148.3 mAh·g⁻¹, the charge capacity of 147.0 mAh·g⁻¹, Coulomb efficiency is 99.1%. In this case, the initial charge-discharge capacity is the highest, and the platform area is also the widest.

Figure 8 shows the 10 cycles of the sample at different sintering temperatures under 0.1C. When heat treatment temperature is 700 °C, the specific capacity of the discharge was reduced from 148.3 mAh·g⁻¹ to 132.5 mAh·g⁻¹ after the 10 cycles of discharge, the capacity retention rate was 89.3%. After heat treatment at 600 °C and 500 °C, the capacity retention rate of the sample was 91.1% and 91.7%, respectively. While the capacity of the sample under 800 °C heat treatment had a larger attenuation, capacity retention rate of which was only 82.3%. It may be due to the particles in the high temperature had a tendency to grow, which made the transmission of Li⁺ during the process of charge and discharge become more difficult. This causes a certain degree of polarization. Which lead to attenuation of discharge capacity.

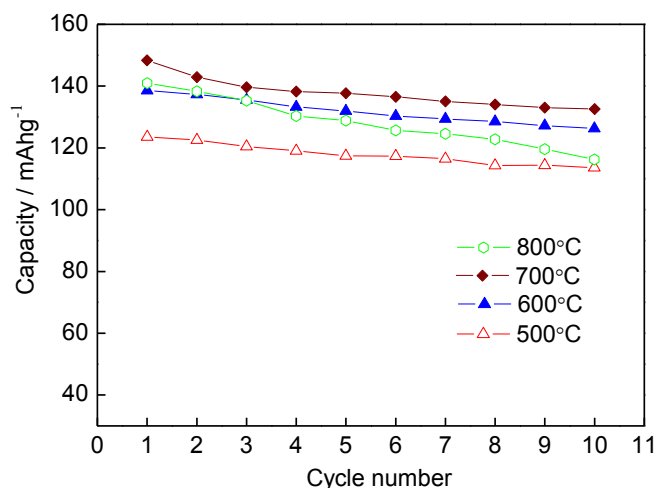


Figure 8. Cycling performance curves for the samples synthesized at different sintering temperatures

4. CONCLUSIONS

1) The spinel Li₄Ti₅O₁₂ microspheres were synthesized by hydrothermal method using tetrabutyl titanate, potassium chloride and lithium hydroxide. When the 0.2 g hydrolyzate was reacted with 2.55 mmol LiOH·H₂O, the heat-treated product was pure phase Li₄Ti₅O₁₂; when hydrothermal at 180 °C for 36 h, the spherical particles get the best development; different heat treatment temperature conditions, the sample volume average particle size is about 400-600 nm, particle size distribution is 100-900 nm;

2) The synthesis process of lithium titanate microspheres may be: in the hydrothermal reaction, Li^+ is replaced with cation in hydrated TiO_2 microspheres, and then $\text{Li}_4\text{Ti}_5\text{O}_{12}$ microspheres are formed by heat treatment;

3) The discharge platform of sample is 1.55 V, the charging platform is 1.60 V, and the reversibility is good; when the heat treatment temperature is 700 °C, the sample has the highest initial discharge specific capacity of $148.3 \text{ mAh}\cdot\text{g}^{-1}$ at 0.1C, After the charge and discharge cycle, the discharge capacity decreased to $132.5 \text{ mAh}\cdot\text{g}^{-1}$, the capacity retention rate was 89.3%.

ACKNOWLEDGEMENTS

The authors make great acknowledgments for the foundation supports NO 51165016 and 51301144.

References

1. N. Nitta, F. X. Wu, J. T. Lee, G. Yushin, *Mater. Today*, 18 (2015) 252.
2. W. N. Chen, H. Jiang, Y. J. Hu, Y. H. Dai, C. Z. Li, *Chem. Commun.*, 50 (2014) 8856.
3. M. Armand, J. M. Tarascon, *Nature*, 451 (2008) 652.
4. J. B. Goodenough, Y. Kim, *Chem. Mater.*, 22 (2010) 587.
5. Q. Zhang, M. G. Verde, J. K. Seo, X. Li, Y. S. Meng, *J. Power Sources*, 280 (2015) 355.
6. B. B. Tian, H. F. Xiang, L. Zhang, H. H. Wang, *Solid State Electrochem*, 16 (2011) 205.
7. C. C. Chen, Y. N. Huang, H. Zhang, X. F. Wang, G. Y. Li, Y. J. Wang, L. F. Jiao, H. T. Yuan, *J. Power Sources*, 278 (2015) 693.
8. X. H. Yu, Z.L. Zhan. *Nanoscale Res. Lett.* 9 (2014) 516.
9. A. K. Haridas, C. S. Sharma, T. N. Rao, *Small*, 11 (2015) 290.
10. G. Y. Liu, H. Y. Wang, G. Q. Liu, Z. Z. Yang, B. Jin, Q. C. Jiang, *J. Power Sources*, 220 (2012) 84.
11. L. Gao, S. H. Li, D. K. Huang, Y. Shen, M. K. Wang, *J. Mater. Chem. A.*, 3 (2015) 10107.
12. A. J. Wei, W. Li, L. H. zhang, X. H. Li, X. Bai, Z. F. Liu, *nano*, 12 (2017) 1750054.
13. H. Song, T. G. Jeong, S. W. Yun, E. K. Lee, S. A. Park, Y. T. Kim, *Sci Rep.*, 7 (2017) 43335.
14. H. C. Chiu, X. Lu, J. G. Zhou, L. Gu, J. Reid, R. Gauvin, K. Zaghbi, G. P. Demopoulos, *Adv Energy Mater.*, 7 (2017) 1601825.
15. X. F. Wang, B. Liu, X. J. Hou, Q. F. Wang, W. W. Li, D. Chen, G. Shen, *Nano Res.*, 7 (2014) 1073.
16. L. F. Shen, E. Uchaker, X. G. Zhang, G. Z. Cao, *Adv Mater.*, 24 (2012) 6502.
17. J. Liu, K. P. Song, P. A. van Aken, J. Maier, Y. Yu, *Nano letters*, 14 (2014) 2597.
18. L. Yu, H. B. Wu, X. W. Lou, *Adv. Mater.*, 25 (2013) 2296.
19. X. H. Yu, Z. L. Zhan, J. Rong, Z. Liu, L. Li, J. X. Liu. *Chem. Phys. Lett.* 600 (2014) 43.
20. Y. F. Tang, L. Yang, S. Fang, Z. Qiu, *Electrochim. Acta*, 54 (2009) 6244.
21. H. Yan, Z. Zhu, D. Zhang, W. Li, Q. Lu, *J. Power Sources*, 219 (2012) 45.
22. N. Zhang, Z. Liu, T. Yang, C. Liao, Z. Wang, K. Sun, *Electrochem. Commun*, 13 (2011) 654.
23. Y. C. Kuo, H. T. Peng, Y. M. Xiao, J. Y. Lin, *J Solid State Electr.*, 6 (2016) 1625.
24. R. Krishnaswamy, A. K. Sood, Growth, *J. Mater. Chem.*, 20 (2010) 3539.
25. X. H. Yu, J. Rong, Z. L. Zhan, Z. Liu, J.X. Liu. *Mater. design.* 83C (2015) 159.
26. C. Kursun, M. Gogebakan, *J. Alloys Comd.*, 619 (2015) 138.
27. G. Y. Liu, R. X. Zhang, K. Y. Bao, H. Q. Xie, S. L. Zheng, J. L. Guo, G. Q. Liu, *Ceram Int.*, 42 (2016) 11468.
28. Y. J. Sha, X. M. Xu, L. Li, R. Cai, Z. P. Shao, *J. Power Sources*, 314 (2016) 18.
29. T. F. Yi, H. Liu, Y. R. Zhu, L. J. Jiang, Y. Xie, R. S. Zhu, *J. Power Sources*, 215 (2012) 258.

30. Y. Tang, L. Yang, S. Fang, Z. Qiu, *Electrochim. Acta*, 54 (2009) 6244.
31. L. F. Shen, C.Z. Yuan, H. J. Luo, X. G. Zhang, L. Chen, H.S. Li, *J. Mater. Chem.*, 21 (2011) 14414.
32. J. Z. Chen, L. Yang, S. H. Fang, Y. F. Tang, *Electrochim. Acta*, 55 (2010) 6596.
33. R. Xu, J. R. Li, A. Tan, Z. L. Tang, Z. T. Zhang, *J. Power Sources*, 196 (2011) 2283.
34. Y. Q. Wang, L. Gu, Y. G. Guo, H. Li, X. Q. He, S. Tsukimoto, Y. Ikuhara, L. J. Wan, *J. Am. Chem. Soc.*, 134 (2012) 7874.
35. X. Wang, J. Rong, Y.M. Song, X.H. Yu, Z.H. Zhan, J.S. Deng, *Phys. Lett. A*, 381 (2017) 2845.
36. Y. C. Li, G. Y. Fu, M. Watson, S. Harrison, M. P. Paranthaman, *ChemNanoMat.*, 2 (2016) 642.
37. H. Y. Wu, M. H. Hon, C. Y. Kuan, L. C. Leu, *Rsc Adv.*, 5 (2015) 35224.
38. H. B. Yin, Y. Wada, T. Kitamura, *J Mater Chem.*, 11 (2001) 1694.
39. Y. W. Wang, H. Xu, X. B. Wang, *J Phys Chem B.*, 110 (2006) 13835.

© 2017 The Authors. Published by ESG (www.electrochemsci.org). This article is an open access article distributed under the terms and conditions of the Creative Commons Attribution license (<http://creativecommons.org/licenses/by/4.0/>).